Real time observer and control scheme for a Wind Turbine System based on a high order sliding modes

Oscar Barambones, José A. Cortajarena, Isidro Calvo, José M. Gonzalez de Durana, Patxi Alkorta and Ali Karami-Mollaee*
University of the Basque Country, (UPV/EHU)
∗ Hakim Sabzevari University, Sabzevar, Iran
Faculty of Engineering of Vitoria-Gasteiz
Nieves cano, 12. 1006 Vitoria-Gasteiz, Spain
oscar.barambones@ehu.eus

Abstract

The introduction of advanced control algorithms may improve considerably the efficiency of wind turbine systems. This work proposes a high order sliding mode (HOSM) control scheme based on the super twisting algorithm for regulating the wind turbine speed in order to obtain the maximum power from the wind. A robust aerodynamic torque observer, also based on the super twisting algorithm, is included in the control scheme in order to avoid the use of wind speed sensors. The presented robust control scheme ensures good performance under system uncertainties avoiding the chattering problem, which may appear in traditional sliding mode control schemes. The stability analysis of the proposed HOSM observer is provided by means of the Lyapunov stability theory. Experimental results show that the proposed control scheme, based on HOSM controller and observer, provides good performance and that this scheme is robust with respect to system uncertainties and external disturbances.

Keywords: Wind Turbine, High order sliding mode, power generation control; Real-time control; DFIG (doubly-fed induction generator).

1. Introduction

Wind power global capacity increased severely from 7.5 GW to 597 GW between the years 1997 and 2018 [1], becoming nowadays one of the most profitable sources of electricity. This trend is expected to continue over the next years by improving the efficiency of the plants and achieving the needed cost-competitiveness ratio [2]. In this scenario, Doubly Feed Induction Generators (DFIG) and vector control techniques are widely applied in variable speed wind turbine control systems, due to their capacity for maximizing wind power extraction at different wind speeds. The control schemes used in DFIG wind turbines should be designed taking into account: the DFIG rotor speed, which must be regulated for extracting the maximum power from the wind; the frequency of the DFIG output voltage, which must be kept constant; and the DFIG reactive power [3]-[7]. The designed controllers should drive the rotor speed of the turbine to the optimal point of operation for maximizing the active power. Unfortunately, this objective is difficult to achieve due to that the wind speed may change abruptly, e.g. in bursts, and that wind turbine systems are inherently non-linear, introducing several uncertainties [8]-[11].

During the last decade, several nonlinear control techniques were introduced to improve the control of wind turbine systems considering its nonlinear nature. In [12], the authors proposed a Neural Input–Output Feedback Linearization controller for a wind turbine connected to the grid with a DFIG. Authors estimated one model, based on a Recurrent High Order Neural Network, which was used to implement the proposed control law. However, implementing this approach in real applications with low-cost real time processors may become difficult, since control schemes based on Neural Networks typically require high computational cost. In [13], a fault tolerant model predictive control scheme was proposed, aimed at working in the partial-load region even in the presence of system uncertainties. The authors validated the control scheme against system uncertainties by means of several simulations but it was not validated in real time. Sliding mode control is a robust and non-linear control technique, especially suited for wind turbine systems due to its recognized robustness to parameters uncertainties and non-linear structure. Furthermore, it can be implemented in real applications, using low-cost real-time processors, since it requires low computational cost. In [14], the authors proposed a coordinated high-order sliding mode control scheme for optimizing the power extraction in a DFIG based system. In this work, the wind energy was maximized by tracking the optimal speed of the rotor with a super-twisting algorithm. However, they needed to measure the speed of the wind to calculate the optimal speed of the rotor.

Typically, anemometers are installed on the top of the nacelle for measuring the wind speed. However, the wind speed varies spatially on the swept rotor area so that it is difficult to obtain an accurate value of the rotor effective wind speed. Moreover, the anemometer increases the system cost, the complexity, the maintenance and reduces the reliability. In [15], a sliding mode control scheme without wind speed measurements was designed for variable speed wind turbines. The objective was to maximize power extraction. In this work the authors proposed a wind speed estimator based on the Newton-Raphson algorithm. However, their estimator was not robust under system uncertainties. Moreover, the proposed control scheme was not validated in real time control platforms. In [16] a sliding mode control scheme was proposed using a novel exponential reaching law. Their approach was aimed at optimizing the power generated by the turbine under variable wind speeds. The exponential reaching law reduced the chattering phenomenon. However, this control scheme required the value of the wind speed to calculate the reference for the electromagnetic torque. In addition, this control scheme was not validated in real-time control platforms.

This paper proposes a robust wind torque observer aimed at avoiding wind speed sensors in variable speed turbines. The observer is based on the High Order Sliding Mode (HOSM) technique [17], [18]. The optimal value for the angular velocity of the turbine rotor can be calculated from the torque value observed. This value is used as reference for the proposed control scheme, so that the control algorithm maximizes power extraction. Additionally, the HOSM theory is used to reduce the chattering phenomenon in the sliding mode control scheme. The proposed HOSM observer and controller are validated experimentally over a real time control platform designed and built ad hoc. The control platform is based on a real commercial DFIG of 7.5 kW, being connected to the real grid so that experimental results can be easily extended to real industrial applications. The control scheme is aimed at maximizing wind power even in the presence of uncertainties in the turbine or abrupt changes in the wind speed. This kind of control schemes do not require high computational cost and therefore they may be implemented effectively in real time wind applications [19]-[21]. Mainly, the proposed control scheme regulates the current of the rotor-side converter (RSC) to track the optimal wind turbine speed. In addition, the torque observer is proposed for calculating the optimal value for the turbine speed. This approach avoids the use of sensors for measuring the speed of the wind and, consequently, reduces the price of the system. This control scheme was initially proposed and simulated in [22]. However, in this previous work the proposed control approach was only validated by means of some simulation results using a simple wind turbine model. This work goes beyond, since it provides experimental results using a real test bench that validate the control approach. Further simulations were carried out using a detailed model of the real system, which represents the dynamics more accurately. The test bench used for carrying out the real time experiments is based on commercial machines, typically used in industrial applications. Real experiments validated the results previously obtained in the simulations, and its application in industrial applications. This is a considerable research advance, since it facilitates its implementation in real industrial applications.

The paper is organized as follows. Section 2 deals with the development of the wind turbine modelling used in this work. In Section 3 a torque observer based in the HOSM is introduced. The stability of the proposed observer is analyzed by means of the Lyapunov theory. Section 4 presents the proposed HOSM control scheme. Section 5 validates the proposed control scheme with diverse experiments. Finally, in Section 6 some concluding remarks are drawn.

2. Wind turbine modelling

In wind turbines the power extraction depends mainly on the following factors: the power of the wind, the efficiency of the wind turbine and the capacity of the machine to adapt to variations in the wind. Typically, the power obtained from a wind turbine is calculated by [23], [24]:

$$P_m(\beta, \lambda, v) = \frac{1}{2} C_p(\beta, \lambda) \rho \pi R^2 v^3 \tag{1}$$

in this expression ρ represents the air density, R the rotor radius, v the speed of the wind. C_p the power efficiency coefficient, which is typically measured or calculated by the manufacturer at several wind speeds. C_p depends on β, which is the pitch angle of the blade, and λ, which is the tip-speed ratio, defined as:

$$\lambda = \frac{R\, w}{v} \tag{2}$$

where w is the rotational speed of the wind turbine. From this expression it may be inferred that if the rotational speed were kept constant, any change in the wind speed would vary the tip-speed ratio, affecting the value of the power coefficient C_p. As a result, the generated power output of the wind turbine would change. Nevertheless, in order to remain in an optimal point of operation, so maximizing the power extraction, the tip-speed ratio could be kept constant by adjusting the speed of the rotor in function of the wind speed variation.

In a simplified way, a wind turbine accounts for these components: an aeroturbine, which transforms the energy from the wind into mechanical movement, a gearbox, aimed at augmenting the rotor speed and reducing the torque, and a generator, which converts mechanical movement into electricity.

Thus, the rotor of the wind turbine turns at w driven by the input torque of the wind, T_m. The transmission output torque, T_t, is connected to the generator, achieving a shaft torque of T_e, which moves the generator with a speed of w_e. Due to the use of gearboxes the rotor and generator speeds are different magnitudes.

The mechanical model for the system is represented by [25]:

$$J_m\dot{w} + B_m w = T_m - T \tag{3}$$
$$J_e\dot{w}_e + B_e w_e = T_t + T_e \tag{4}$$
$$T_t w_e = T w \tag{5}$$

In these expressions, J_m and J_e represent respectively the moments of inertia for turbine and generator, B_m and B_e are the viscous friction coefficients for turbine and generator, T_m is the mechanical torque at the turbine, due to the wind, T and T_t are respectively the torque at both sides of the gearbox, T_e is the torque at the generator, w is the angular velocity of the turbine shaft and w_e is the rotational velocity of the generator rotor.

The gear ratio, η, relates the angular velocities of the turbine w and generator w_e:

$$\eta = \frac{w_e}{w} \tag{6}$$

The mechanical model may be compacted by combining equations 3, 4, 5 and 6:

$$J\dot{w} + Bw = T_m + \eta T_e \tag{7}$$

where $J = J_m + \eta^2 J_e$ and $B = B_m + \eta^2 B_e$

Finally, the input torque due to the wind can be obtained by combining equations (1) and (2):

$$T_m(w, \lambda, \beta) = \frac{P_m(\frac{Rw}{\lambda}, \lambda, \beta)}{w} = k_w \cdot w^2 \tag{8}$$

being

$$k_w = \frac{1}{2}\, C_p(\lambda, \beta)\, \rho\, \pi \frac{R^5}{\lambda^3}$$

3. Torque observer for the control scheme

Most control schemes use the measured wind velocity in order to obtain the optimal value for the rotational velocity of the wind turbine. However, observers may be useful to estimate the effective wind speed without using proper sensors [27], [28]. This section presents the aerodynamic torque observer used at the proposed control scheme in order to get the optimal point of operation.

The torque of the wind, T_m, may be considered as a quasi constant magnitude, since the changes in the wind torque may be assumed to happen at specific time instants. Mathematically this is represented by a null derivative. Thus, from eqn.(7) the system state space equations for the wind turbine can be written as:

$$\begin{aligned} \dot{w} &= \frac{1}{J}\left(T_m - Bw + \eta T_e\right) \\ \dot{T}_m &= 0 \end{aligned} \tag{9}$$

Several techniques have been developed in order to avoid the chattering phenomena that may appear in wind turbine systems. One of most popular techniques specifically designed for this purpose is the so-called super-twisting algorithm, which is a second order sliding mode algorithm [29], [30]. This technique, included in the presented control scheme, has been used at the design of the torque observer. Based on this technique, the following algorithm is proposed:

$$\begin{aligned} \dot{\hat{w}} &= \frac{\hat{T}_m}{J} - \frac{B}{J}w + \frac{\eta T_e}{J} - h_1|\hat{w} - w|^{\frac{1}{2}}\,\mathrm{sgn}(\hat{w} - w) \\ \dot{\hat{T}}_m &= -J \cdot h_2\;\mathrm{sgn}(\hat{w} - w) \end{aligned} \tag{10}$$

where h_1 and h_2 are positive values. Let be $e_1 = \hat{w} - w$ the error observed at the angular velocity and $e_2 = \frac{\hat{T}_m}{J} - \frac{T_m}{J}$ the error observed at the torque.

Then, the derivatives of e_1 and e_2 are respectively $\dot{e}_1 = \dot{\hat{w}} - \dot{w}$ and $\dot{e}_2 = \frac{\dot{\hat{T}}_m}{J} - \frac{\dot{T}_m}{J}$. The observation error may be obtained by subtracting eqn.(10) from eqn.(9):

$$\begin{aligned} \dot{e}_1 &= e_2 - h_1|e_1|^{\frac{1}{2}}\,\mathrm{sgn}(e_1) \\ \dot{e}_2 &= -h_2\;\mathrm{sgn}(e_1) \end{aligned} \tag{11}$$

Theorem 1. *Consider the wind turbine system given by eqn.(9) and the HOSM observer given by eqn.(10). Then, if the observer gains h_1 and h_2 are adequately selected as positive values, the estimation errors of the proposed HOSM observer converges to zero.*

Proof To prove the stability of the observer, based on the second order sliding mode technique, the following candidate Lyapunov function is proposed:

$$V = 2\,h_2|e_1| + \frac{1}{2}e_2^2 + \frac{1}{2}\left(h_1|e_1|^{\frac{1}{2}}\,\mathrm{sgn}(e_1) - e_2\right)^2 \tag{12}$$

which can be expressed in the form

$$V = \xi^T P \xi \tag{13}$$

where

$$\xi^T = \begin{bmatrix} |e_1|^{\frac{1}{2}} \operatorname{sgn}(e_1), & e_2 \end{bmatrix}, \quad P = \frac{1}{2} \begin{bmatrix} 4h_2 + h_1^2 & -h_1 \\ -h_1 & 2 \end{bmatrix} \tag{14}$$

By deriving expression (13) with respect to time

$$\dot{V} = \xi^T P \dot{\xi} + \dot{\xi}^T P \xi \tag{15}$$

in which $\dot{\xi}^T$ is obtained from (14) and (11)

$$\begin{aligned}
\dot{\xi}^T &= \left[-\frac{h_1}{2} \operatorname{sgn}(e_1) + \frac{1}{2|e_1|^{\frac{1}{2}}} e_2, \quad -h_2 \operatorname{sgn}(e_1) \right] \\
&= \frac{1}{2|e_1|^{\frac{1}{2}}} \left[-h_1 |e_1|^{\frac{1}{2}} \operatorname{sgn}(e_1) + e_2, \quad -2h_2 \, |e_1|^{\frac{1}{2}} \operatorname{sgn}(e_1) \right] \\
&= \frac{1}{2|e_1|^{\frac{1}{2}}} \begin{bmatrix} -h_1 & 1 \\ -2h_2 & 0 \end{bmatrix} \begin{bmatrix} |e_1|^{\frac{1}{2}} \operatorname{sgn}(e_1) \\ e_2 \end{bmatrix} \\
&= A \xi
\end{aligned} \tag{16}$$

with

$$A = \frac{1}{2|e_1|^{\frac{1}{2}}} \begin{bmatrix} -h_1 & 1 \\ -2h_2 & 0 \end{bmatrix}$$

The following expression is obtained by substituting (16) in (15)

$$\dot{V} = \xi^T P A \xi + \xi^T A^T P \xi = \xi^T (P A + A^T P) \xi \tag{17}$$

Now, in order to arrange the expression, the matrix products

$$\begin{aligned}
PA &= \frac{1}{2} \begin{bmatrix} 4h_2 + h_1^2 & -h_1 \\ -h_1 & 2 \end{bmatrix} \frac{1}{2|e_1|^{\frac{1}{2}}} \begin{bmatrix} -h_1 & 1 \\ -2h_2 & 0 \end{bmatrix} \\
&= \frac{1}{4|e_1|^{\frac{1}{2}}} \begin{bmatrix} -4h_1 h_2 - h_1^3 + 2h_1 h_2 & 4h_2 + h_1^2 \\ h_1^2 - 4h_2 & -h_1 \end{bmatrix}
\end{aligned}$$

and

$$\begin{aligned}
A^T P &= \frac{1}{2|e_1|^{\frac{1}{2}}} \begin{bmatrix} -h_1 & -2h_2 \\ 1 & 0 \end{bmatrix} \frac{1}{2} \begin{bmatrix} 4h_2 + h_1^2 & -h_1 \\ -h_1 & 2 \end{bmatrix} \\
&= \frac{1}{4|e_1|^{\frac{1}{2}}} \begin{bmatrix} -h_1^3 - 4h_1 h_2 + 2h_1 h_2 & h_1^2 - 4h_2 \\ 4h_2 + h_1^2 & -h_1 \end{bmatrix}
\end{aligned}$$

are calculated

$$PA + A^T P = \frac{2}{4|e_1|^{\frac{1}{2}}} \begin{bmatrix} -h_1^3 - 2h_1 h_2 & h_1^2 \\ h_1^2 & -h_1 \end{bmatrix}$$
$$= -\frac{h_1}{2|e_1|^{\frac{1}{2}}} \begin{bmatrix} h_1^2 + 2h_2 & -h_1 \\ -h_1 & 1 \end{bmatrix}$$
$$= -\frac{h_1}{2|e_1|^{\frac{1}{2}}} Q$$

where

$$Q = \begin{bmatrix} h_1^2 + 2h_2 & -h_1 \\ -h_1 & 1 \end{bmatrix}$$

Thus, the derivative of the Lyapunov function candidate may be expressed as

$$\dot{V} = -\frac{h_1}{2|e_1|^{\frac{1}{2}}} \xi^T Q \xi \tag{18}$$

This function is negative semidefinite since $\dot{V} \leq 0$ if $Q > 0$, and here $Q > 0$ because the two leading principal minors, $(h_1^2 + 2h_2)$ and $\begin{vmatrix} h_1^2+2h_2 & -h_1 \\ -h_1 & 1 \end{vmatrix}$, are positive since h_1 and h_2 are positive values.

Hence, it may be concluded that the estimation error of the proposed observer converges to zero. Thus, it is possible to use this torque observer for calculating the optimal speed reference for the wind turbine, by mweans of eqn.(8) as proposed in the next section.

4. HOSM control scheme for wind turbines

The proposed control scheme is aimed at maximizing the power extraction in DFIG wind turbines. More precisely, the controller adapts the rotational speed of the wind turbine according to the variations in the speed of the wind, so that the optimal value for the tip-speed ratio, λ_{opt}, is enforced. Thus, the extraction of wind energy is maximized. DFIG wind turbines are controlled by regulating the variable frequency converter (VFC), which involves the control of the rotor-side converter (RSC) and the grid-side converter (GSC) [31]. The RSC is responsible for controlling the stator-side active and reactive powers in an independent way whereas the GSC keeps constant the DC-link voltage regardless of the power magnitude and direction of the rotor [26]. Also, the GSC controller regulates the reactive power of the stator terminal voltage. Figure 1 shows an illustrative diagram for this HOSM control scheme for a DFIG based wind turbine.

DFIG wind turbines were designed to operate at different wind speeds while maximizing the extraction of energy. But to achieve it, the speed of the shaft needs to be adjusted according to the optimal tip-speed ratio λ_{opt}, which gets the maximum power coefficient $C_{p_{max}}$ and, consequently, maximizes energy extraction [32]. This implies

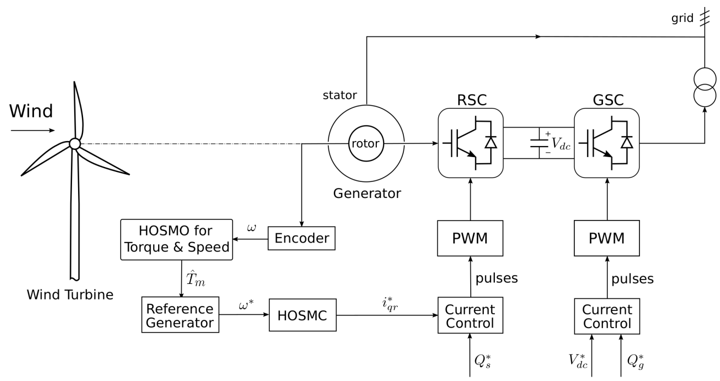

Figure 1: DFIG based wind turbine diagram

that depending on the speed of the wind, the maximum extraction of energy from the wind is achieved by driving the speed of the wind turbine to a specific and unique value. This value is denoted as λ_{opt} which is the maximum value of the power coefficient curves $C_{p_{max}}$ versus the tip-speed ratio. Both the maximum power coefficient curves, $C_{p_{max}}$, and the optimal tip-speed ratio, λ_{opt}, are constructive parameters of the wind turbine.

An approximated model for the power coefficient C_p of a wind turbine was presented in [33]. The equation of this model, which includes the parameters of the turbine, is (19):

$$C_p(\lambda, \beta) = c_1 \left(\frac{c_2}{\lambda_i} - c_3\beta - c_4 \right) e^{\frac{-c_5}{\lambda_i}} + c_6\lambda \tag{19}$$

where c_1, c_2, c_3, c_4, c_5 and c_6 are constructive coefficients of the wind turbine, design dependent. λ_i can be obtained from:

$$\frac{1}{\lambda_i} = \frac{1}{\lambda + 0.08\beta} - \frac{0.035}{\beta^3 + 1} \tag{20}$$

The control algorithm proposed in this work is based on estimated measures of the aerodynamic torque observer, $\hat{T}_m$, for calculating the turbine speed reference. Thus, the optimal aerodynamic torque may be obtained by means of eqn.(8):

$$T_m = k_{w_{opt}} \cdot w_{opt}^2 \tag{21}$$

where

$$k_{w_{opt}} = \frac{1}{2}\, C_p(\lambda_{opt}, \beta)\, \rho\, \pi \frac{R^5}{\lambda_{opt}^3}$$

being λ_{opt} the value of λ that gets the maximum power coefficient C_p.

From this equation and the estimated torque, it can be obtained the optimal value for the angular velocity of the rotor, w_{opt}

$$w^* = w_{opt} = \sqrt{\frac{\hat{T}_m}{k_{w_{opt}}}} \tag{22}$$

This value, w_{opt}, will be used as reference for the controller of the turbine.

In order to maximize the power extraction from the wind, in the presented approach the Rotor Side Control is aimed at driving the wind turbine to turn at this value, w_{opt}. In DFIG-based generation systems this may be enforced by controlling the current at the rotor of the electrical generator.

Frequently, vector control theory is used to simplify the equations that model DFIG systems. Vector control theory represents the stator currents of the machine as a vector with two components, d and q, respectively related to the magnetic flux and torque of the machine. Thus, by using this reference frame, the stator flux linkage vector, ψ_s, and the d-axis are aligned, so that ψ_{ds}=ψ_s and ψ_{qs}=0. The model for the machine may be expressed as [8]:

$$i_{qs} = -\frac{L_m i_{qr}}{L_s} \tag{23}$$

$$i_{ds} = \frac{L_m(i_{ms} - i_{dr})}{L_s} \tag{24}$$

$$i_{ms} = \frac{v_{qs} - r_s i_{qs}}{w_s L_m} \tag{25}$$

$$T_e = -\frac{3p}{4}\frac{L_m^2 i_{ms} i_{qr}}{L_s} \tag{26}$$

$$Q_s = \frac{3}{2}\frac{w_s L_m^2 i_{ms}(i_{ms} - i_{dr})}{L_s} \tag{27}$$

$$v_{dr} = r_r i_{dr} + \sigma L_r \frac{di_{qr}}{dt} - sw_s \sigma L_r i_{qr} \tag{28}$$

$$v_{qr} = r_r i_{qr} + \sigma L_r \frac{di_{qr}}{dt} + sw_s \left(\sigma L_r i_{dr} + \frac{L_m^2 i_{ms}}{L_s}\right) \tag{29}$$

where L_r and L_s are the inductances of rotor and stator respectively, L_m the mutual inductance, w_s the synchronous velocity at the rotor, w_e the rotor speed of the generator, $sw_s = w_s - w_e$ the slip frequency, p the number of poles and $\sigma = 1 - \frac{L_m^2}{L_s L_r}$.

The stator magneizing current, i_{ms}, may be regarded constant due to that the stator is directly connected to the grid and that the stator introduces a small resistance [26]. Thus, the following expression may be used to represent the electromagnetic torque:

$$T_e = -K_T i_{qr} \tag{30}$$

note that K_T is a constant value defined as:

$$K_T = \frac{3p}{4}\frac{L_m^2 i_{ms}}{L_s} \tag{31}$$

By substituting eqn. (30) in eqn.(7) it may be observed that the q-axis rotor current component, i_{qr}, may be used to regulate the speed of the wind turbine, w, according to the dynamic equation (32), whereas the d-axis rotor current component, i_{dr} may be used to regulate the stator reactive power, Q_s (See eqn. (27)).

$$\dot{w} = \frac{1}{J}\left(T_m - \eta K_T i_{qr} - Bw\right) \tag{32}$$

The speed tracking error was defined as:

$$e_w(t) = w(t) - w^*(t) \tag{33}$$

where w^* is the reference for the speed of the rotor.

The following expression is obtained after deriving with respect to time previous expression for $e_w(t)$.

$$\begin{aligned} \dot{e}_w(t) &= \dot{w} - \dot{w}^* \\ &= \frac{T_m}{J} - \frac{\eta K_T}{J} i_{qr} - \frac{B}{J} w - \dot{w}^* \\ &= -H i_{qr} + G \end{aligned}$$

in which H and G were defined as:

$$\begin{aligned} H &= \frac{\eta K_T}{J} \\ G &= \frac{T_m}{J} - \frac{B}{J} w - \dot{w}^* \end{aligned}$$

Assuming that the system uncertainties of the wind turbine are bounded by:

$$\begin{gathered} 0 < \Gamma_m \leq H \leq \Gamma_M \\ |\dot{G}| < \Phi \end{gathered}$$

Note that these assumption just mean that H has positive finite lower and upper bounds and that $|\dot{G}|$ is bounded.

The following expression for the second derivative of the speed tracking error can be obtained.

$$\ddot{e}_w = -H \dot{i}_{qr} + \dot{G} \tag{34}$$

Typically, the use of sliding mode control schemas introduces the chattering phenomena, basically due to the abrupt discontinuities introduced by the control signal. In order to avoid or, at least, reduce this kind of phenomena some approaches, like high order sliding modes and the supertwisting algorithm [34]-[38], were proposed in the literature. Herein the following control approach is proposed, based on the supertwisting algorithm [34]:

$$
\begin{aligned}
i_{qr} &= u + k_1|e_w|^{1/2}\,\mathrm{sgn}(e_w) && (35)\\
\dot{u} &= k_2\,\mathrm{sgn}(e_w) && (36)
\end{aligned}
$$

According to [34], the parameters of the controller must fulfill the following sufficient conditions to guarantee the convergence of the approach in finite time, i.e. that the error at the speed of the turbine is zero, $e_w = 0$:

$$
\begin{aligned}
k_1 &> \frac{\Phi}{\Gamma_m} && (37)\\
k_2^2 &> \frac{4\Phi}{\Gamma_m^2}\frac{\Gamma_M(k_1+\Phi)}{\Gamma_m(k_1-\Phi)} && (38)
\end{aligned}
$$

Consequently, it may be concluded that the proposed controller for the velocity, based on the HOSM algorithm, is adequate since it allows the tracking of the turbine speed and maximize the power extraction even when there are uncertainties in the system. In addition, the presented approach allows the achievement of maximum wind power extraction for all the speed values that may appear over time.

5. Experimental Results

This section analyses the performance of a variable speed wind turbine when the proposed HOSM control scheme is applied. The objective of this controller is to maximize wind power extraction in order to obtain the maximum electrical power, hence, the wind turbine speed must be adjusted continuously against wind speed.

5.1. Experimental test rig

The test rig used to analyse the performance of the proposed control scheme is shown in figure (2). The control algorithms were implemented over a PC running MatLab7/Simulink R2007a, dsControl 3.2.1 software packages, equipped with a DS1103 Controller Board, a real-time interface provided by dSpace. This board is based on a 1 GHz floating point PowerPC processor.

The Doubly Feed Induction Machine (DFIM) was implemented with a 7.5 kW, 1447 rpm, commercial generator, supplied by Leroy Somer. Table 1 summarizes most relevant parameters.

The electrical generator was connected to the electrical network in a Back to Back configuration, implemented by means of two VSI (Voltage Source Inverters). The mechanical torque generated by the wind turbine was emulated by means of a PMSM (Permanent Magnet Synchronous Machine) of 10.6 kW. The rotor speed for these electrical machines was measured using the incremental encoder of the PMSM, of 4096 PPR (Pulses Per Revolution). In order to ensure protection against overcurrents, the rotor and stator currents were software bounded at nominal values. The values of the stator and rotor currents, AC and DC voltages and speed obtained from the sensors were adapted in hardware and connected to the dSpace board. The DS1103 Controller

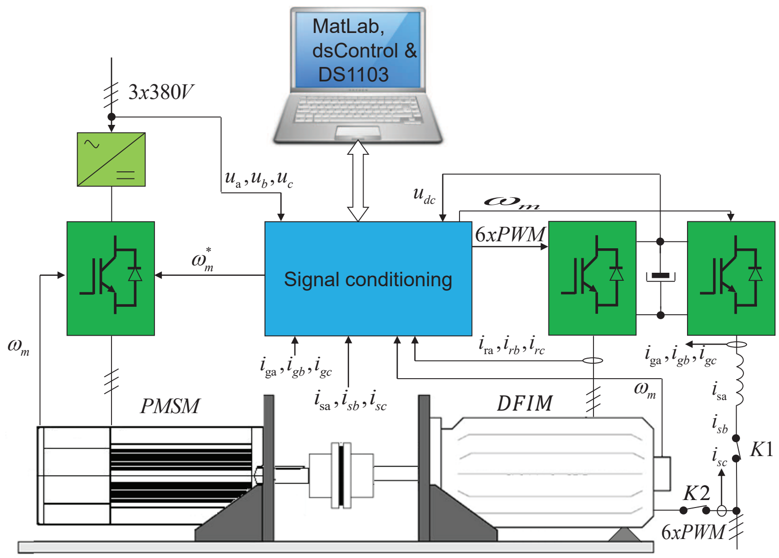

Figure 2: Doubly Fed Induction Machine test rig

Stator Voltage	380 V
Rotor Voltage	190 V
Rated stator current	18 A
Rated rotor current	24 A
Rated speed	1447 r.p.m.@ 50 Hz
Rated torque	50 Nm
Stator resistance	0.42 Ω
Rotor resistance	0.14 Ω
Magnetizing inductance	0.063 H
Stator leakage inductance	0.0018 H
Rotor leakage inductance	0.0023 H
Inertia moment	0.120 Kg.m^2
Viscous friction coefficient	0.005 N.m.s

Table 1: Ratings and parameters of the DFIG (Leroy Somer).

Board drove both inverters providing the SVPWM (Space Vector Pulse Width Modulation) pulses. The SVPWM frequency was set to 10 kHz. This frequency determines the sampling period for the execution of the control algorithm, which was set at 100 μs. The inverters dead time were software fixed to 1 μs. In order to get the module and angle of the grid voltage vector, a synchronous reference frame phase-locked loop

(SRF-PLL) was employed. The grid converter was governed in the grid voltage reference system, by means of a DC signal of 580 V and 0 VA. Conventional PIs with anti-windup are used as current controllers for the experimental validation.

The test rig, which was designed and constructed in order to carry out the experimental validation, is shown in figure 3. In this figure the PMSM, which provides the mechanical torque to the DFIM, is coupled to the DFIM, as it can be appreciated. The figure also shows the RSC and the GSC, located inside the inverter cabinet, as well as the control PC where the software to interact with dSpace DS1103 real-time controller board is run.

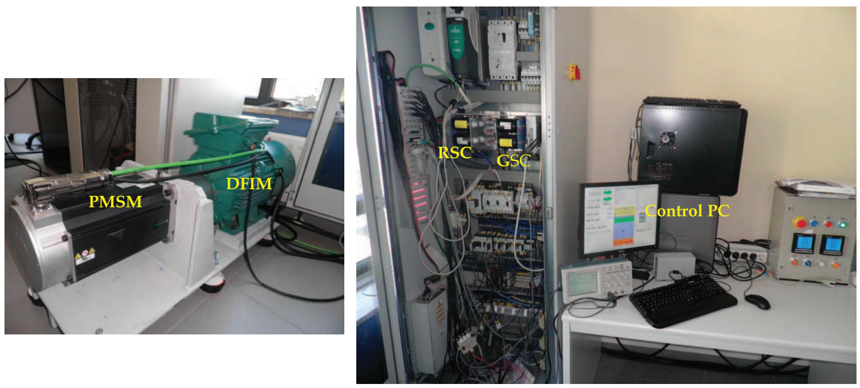

Figure 3: Photography of the experimental platform

5.2. Wind turbine system simulation and experimental validation

This subsection is aimed at validating the Matlab/Simulink simulation model involving the plant and control scheme with the experimental behaviour of the platform itself. For this purpose, several tests were performed and the results of the simulation model and experimental platform were compared. Thus, the measurements taken in the real system with a LeCroy 104Xi oscilloscope were compared with the simulations performed in the system model. The first test was carried out for 10 seconds. In this test the DFIG speed was changed in steps while the load torque also changed as shown in Figures 4 and 5. In order to appreciate in detail these signals, Figures 6 and 7 show the zoom of these figures respectively. It can be observed the similarity between the real measured and simulated signals.

Figures 8 and 9 depict the active and reactive powers at both stator and rotor measured at the test rig as well as those obtained from the simulation model respectively. Again, it can be observed the similarity between the real measured and simulated signals. These figures were taken as validation of the simulation model developed for the test rig.

Finally, figures 10 and 11 show the stator voltage and current phase and rotor current phase for the experimental platform and simulation model respectively when in-

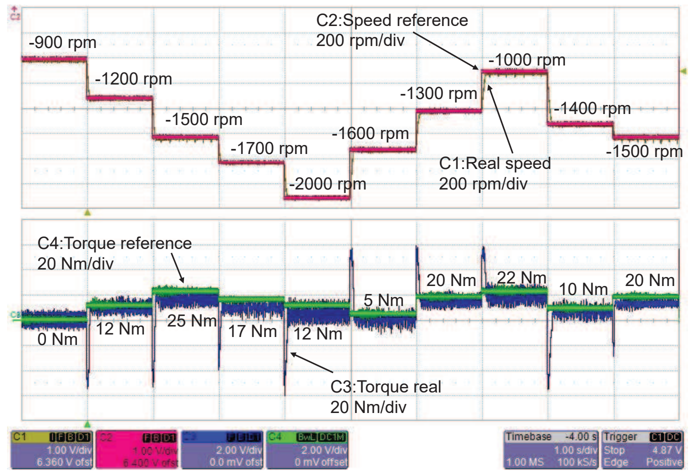

Figure 4: Test rig experimental results

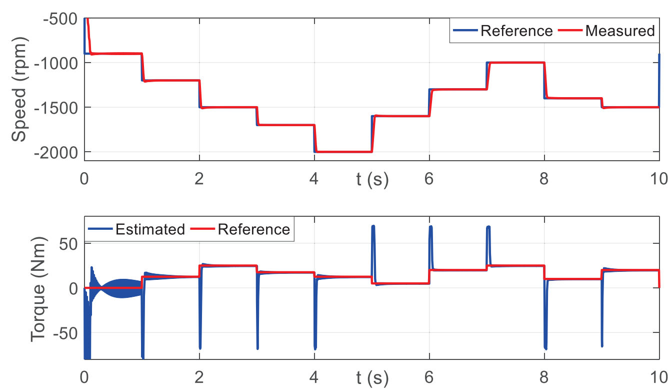

Figure 5: Platform model simulation results

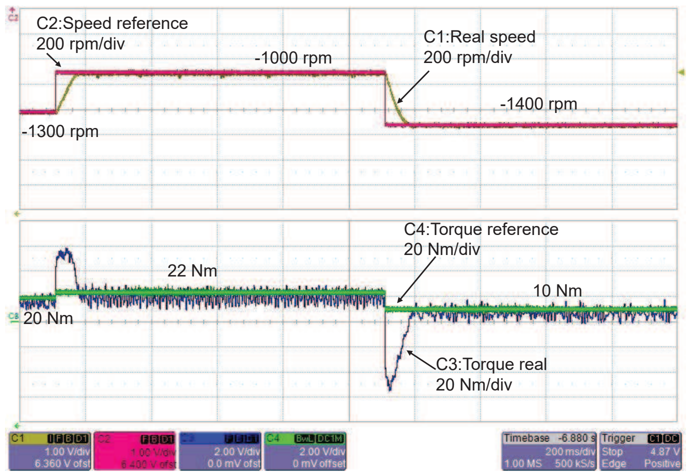

Figure 6: Test rig experimental results

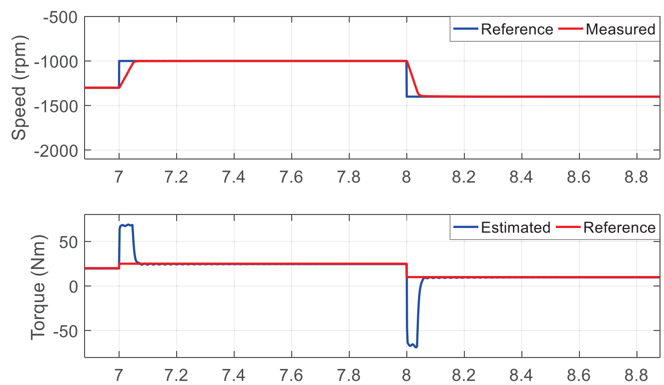

Figure 7: Platform model simulation results

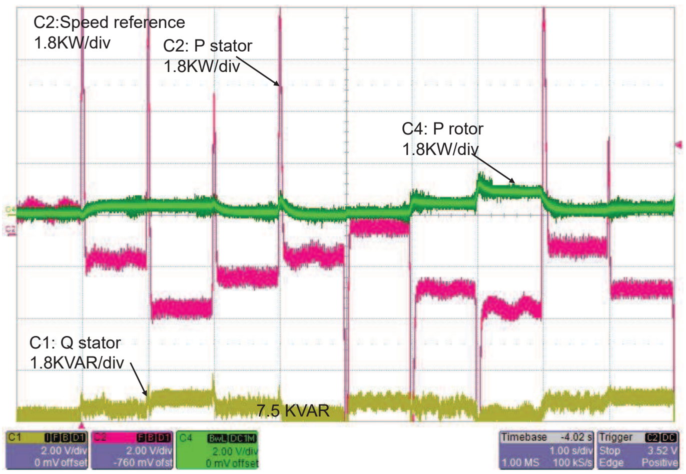

Figure 8: Active and reactive stator powers and rotor active power measured at the experimental platform

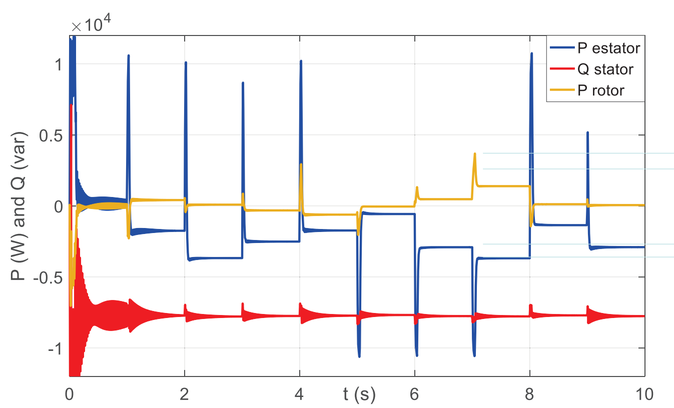

Figure 9: Active and reactive stator powers and rotor active power obtained from the simulation model

jected an active power of 7kW and 0 kVA into the grid. The generator speed was 1660rpm at this experiment. Taking into account this value and considering a synchronous speed of 1500 rpm and two pair poles, the rotor current frequency was 5.5Hz. The amplitude of the rotor current was 50 A and, consequently, the power injected into the grid by the rotor was 400 W.

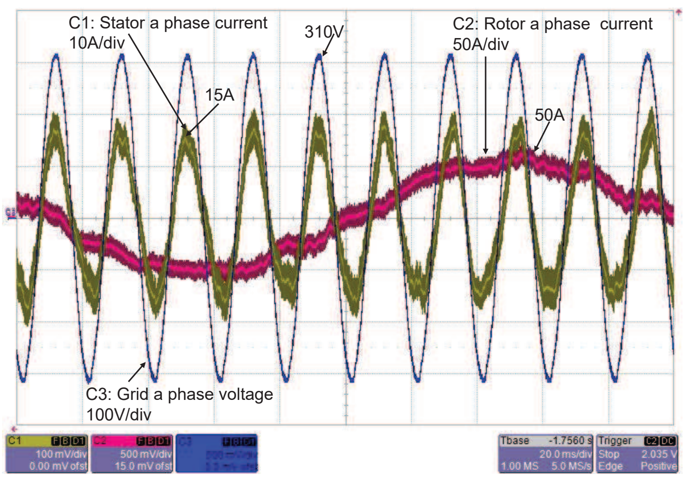

Figure 10: Stator voltage and current phase and rotor current phase measured at the experimental platform

As it can be observed at the previous experiments all the comparisons presented between the real system and the simulation model verify that the developed model emulates accurately the experimental. Consequently, the system model can be used to get, in advance, a preliminary version of the real system response using the control scheme presented in this article, based on the real time observer and slide mode control techniques. Thus, the simulation model allows accelerating the process of tuning the controller tune while avoiding the implementation of control schemes that could damage the experimental platform.

5.3. Sliding torque estimator and reference signal

Equation (26) determines the electrical torque generated in the DFIG by the mechanical torque produced due to the wind speed. Next experiment is devoted to check the performance of the presented sliding mode observer. Thus, the double feed induction machine speed and torque were compared with its estimated values. Both, the torque generated by the wind in the machine and the speed were estimated using the observer proposed in equation (10). The values of the constants h_1 and h_2 were pre-adjusted using the simulation model and tuned more accurately in the experimental platform. The following values were set for this experiment, $h_1 = 10$ and $h_2 = 10$.

In order to test whether the control scheme is suitable for operating conditions, a real wind speed profile was used. These data were measured in a meteorological station located in Salt Lake City (situated in the northern part of the U.S. state of Utah) at a

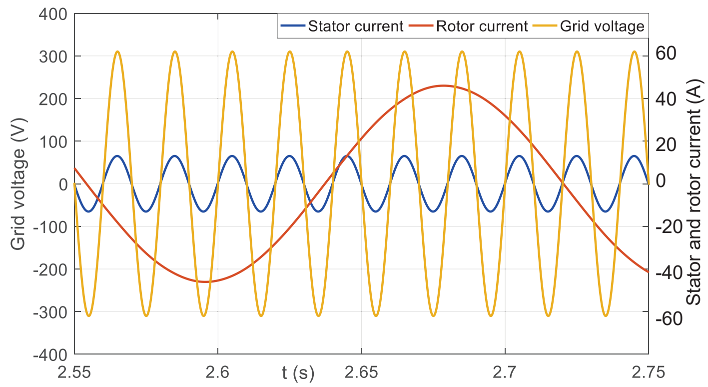

Figure 11: Stator voltage and current phase and rotor current phase obtained from the simulation model

height of 10 m [39]. The profile was depicted in figure 12. The velocity values of the wind profile were used to check the torque and velocity estimator proposed in this work. These values were taken in a $100s$ interval using a period of $1s$. Obviously, such a large period may cause sudden transitions of the velocity. However, in spite of these sudden transitions, the proposed speed estimator presents a good response as shown in the figure 12. The similarity between the real and estimated torque values can be appreciated in figure 13.

According to equation (22), the estimated torque can be used to generate the speed reference to the DFIG, thus obtaining the maximum power from the wind. The estimator of torque and speed depend on J and B, as shown in equation (10). Therefore, in order to observe the robustness of the estimator to errors in these parameters, several tests were performed with different errors in the J value at several conditions for the values of speed and torque.

Figure 14 shows the performance of the observer when the estimator uses the real value for the inertia moment. As it can be observed, both speed and torque were accurately estimated. In the following test, presented in figure 15, the inertia moment used at the estimators was 25% greater than the real one. In the experiment presented in figure 16, the inertia moment used in the estimators was 25% lower than the real one. As it can be observed in these figures, the speed estimation suffers hardly any degrada-

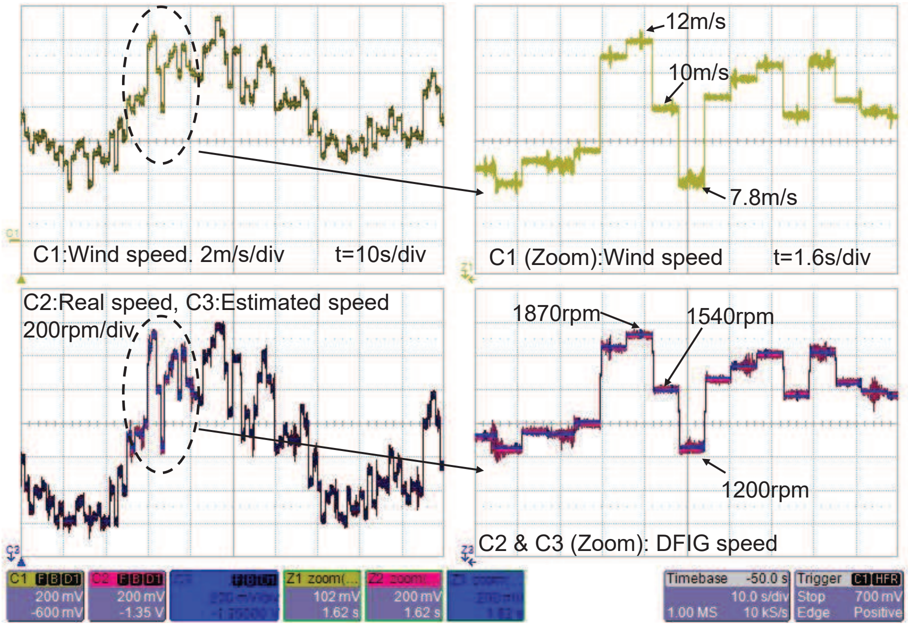

Figure 12: Measured and estimated rotor mechanical speed in the DFIG

tion, however, the estimated torque, although correct in stationary regime, suffers some degradation under abrupt changes as shown in figures 15 and 16.

5.4. *Control algorithm*

This subsection is aimed at testing the performance of the proposed HOSM controller with the proposed HOSM estimator by means of several experiments carried out in the test rig. For this test the real wind speed profile shown in figure 14, which as mentioned in subsection 5.3 it was measured in the Salt Lake Basin, was used. The values for the speed sliding controller were adjusted firstly in simulation and later slightly modified at the experimental platform in order to improve the system response. Thus, the parameters obtained of equations (35) and (36) were $k_2 = 400$ and $k_1 = 70$. Figure 17 shows the obtained stator, rotor and total active powers for the mentioned wind profile. The reactive power was fixed to 4 kVA and the active power was changing to get the maximum power according to equation (22).

When the wind speed was higher than 10m/s, that is, the speed of the machine was 1500rpm or synchronous speed, the rotor power flow went to the grid (negative power). In the remaining situations, the machine turned below the synchronous speed, and the power was absorbed from the grid through the rotor (positive power). The obtained average rotor power was 0,67kW, the stator average was -3,16kW, which is the total power obtained from the machine -2.49kW (including both rotor and stator power).

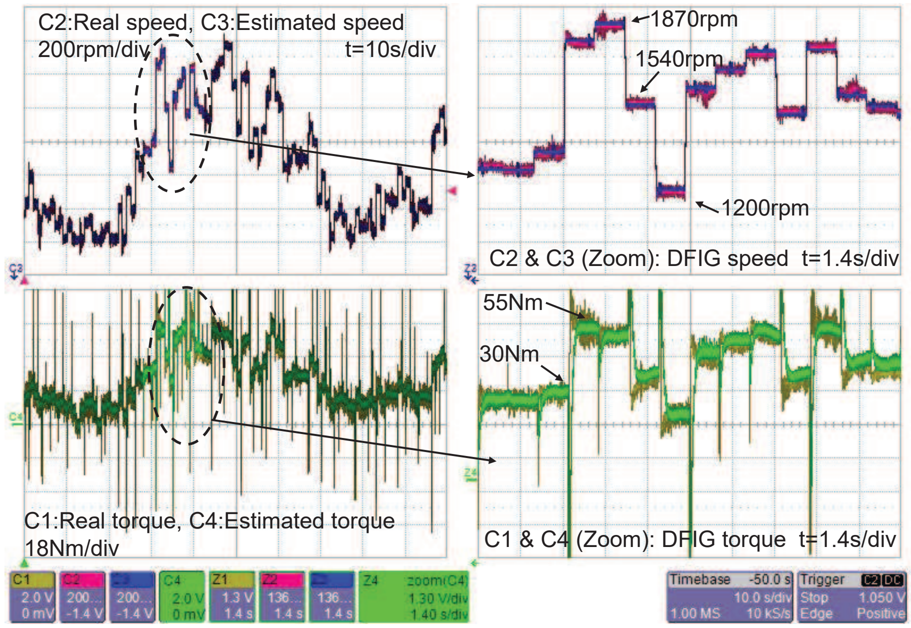

Figure 13: Measured and estimated torque in the DFIG

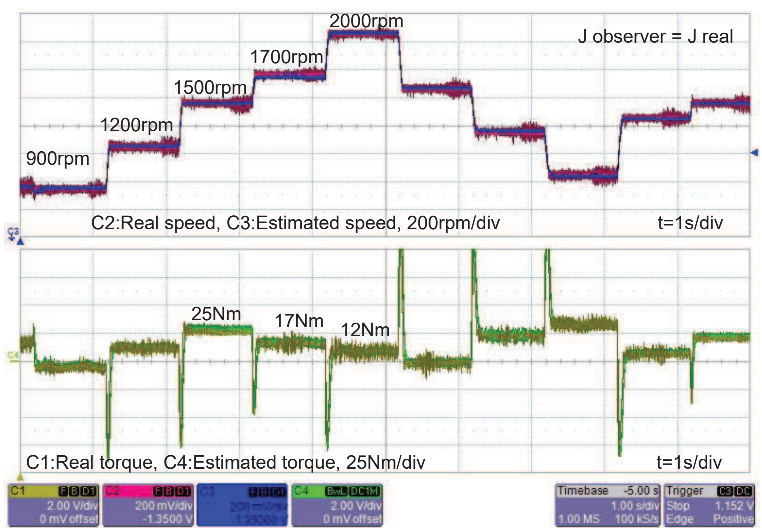

Figure 14: Real and estimated speed and torque for real J value

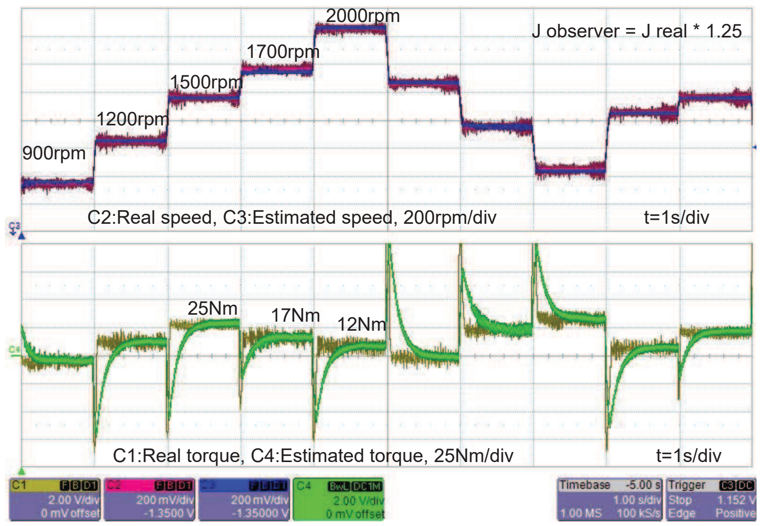

Figure 15: Real and estimated speed and torque for +25% real J value

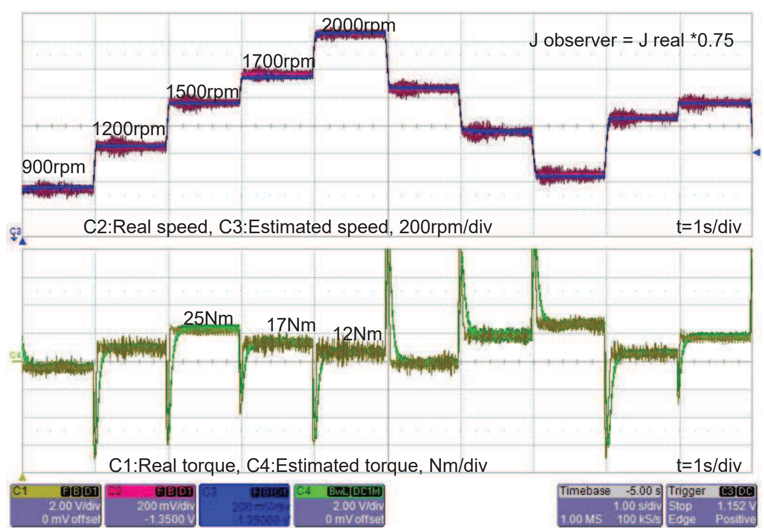

Figure 16: Real and estimated speed and torque for -25% real J value

Figure 18 shows the machine stator and rotor currents for the test wind profile, shown in figure 12. The rotor and stator currents are proportional but the frequency of the rotor is changing according to the slip speed. This change in the frequency can be seen in the zoom of the rotor current.

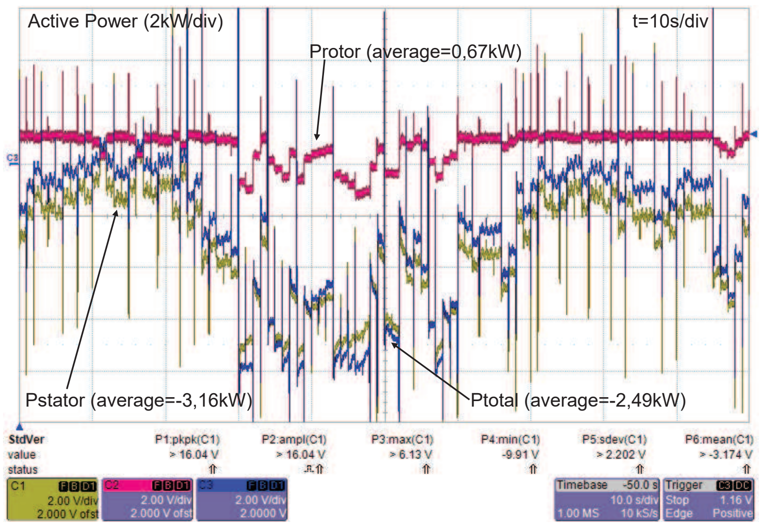

Figure 17: Active powers with the HOSM speed controller for a real wind profile obtaining the maximum power.

5.5. HOSM Control scheme versus PID control

For validation purposes, this section compares the performance of the proposed HOSM Control scheme with a traditional PID controller by means of experimental results. Since the PID controller is the most widely used controller in the industry, this kind of controllers is typically employed as benchmark comparison for new control schemes. For the experimental validation, the PI controller was adjusted for a bandwidth of 75 rad/s and a phase margin of 80 deg. The parameters of the DFIG system were shown in Table 1.

The validation was carried out over the experimental platform designed by the authors. The performance was evaluated using a step change in the wind speed, shown in Figure 19, in order to compare the behavior of the controllers under sudden wind changes, which is a quite demanding task for the control scheme. The wind step variation produces a change in the rotor speed reference, to obtain the maximum power extraction, as shown in Figure 20. This Figure shows the response for both controllers. It can be observed that, if the PID speed controller is adjusted using the calculated plant values, the performance of this controller is a little worse than the performance obtained using the proposed HOSM scheme. As it can be seen, both controllers present a similar rising time but the PID controller presents a small overshoot and, therefore, the system needs more time to reach the new speed reference value, which provides the maximum power extraction from the new wind speed value. This overshoot can be reduced decreasing the proportional action and/or increasing the derivative action, but this would produce a slower response. Obviously due to the system mechanical inertia, the rotor speed cannot track the steep changes in the reference speed instantly, but after

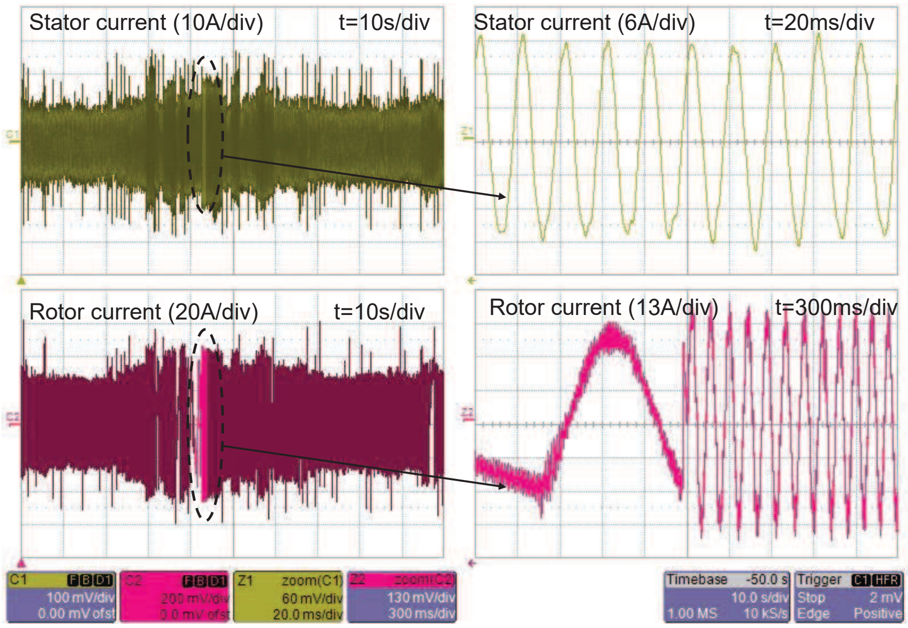

Figure 18: Stator and rotor currents for the real wind profile.

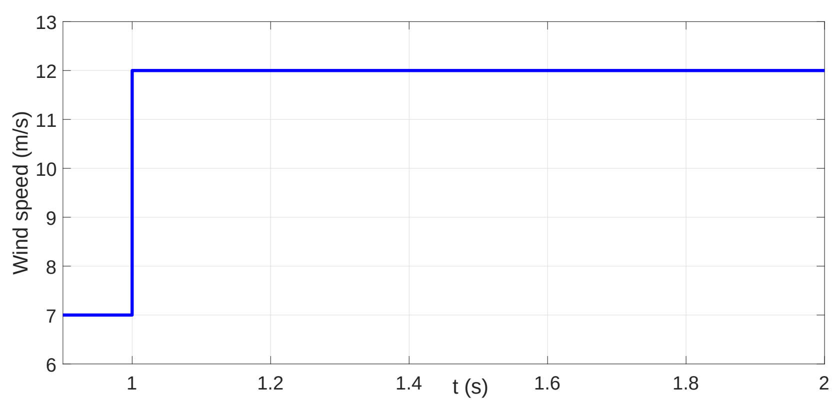

Figure 19: Wind speed step reference

0.13 seconds the reference speed is reached.

In order to compare the robustness of the proposed control scheme, the inertia value of the wind turbine system was increased by means of an inertia wheel, which was added to our control platform. This inertia wheel produces an increase of 25% in the whole value of the system inertia. Figure 21 shows the experimental results ob-

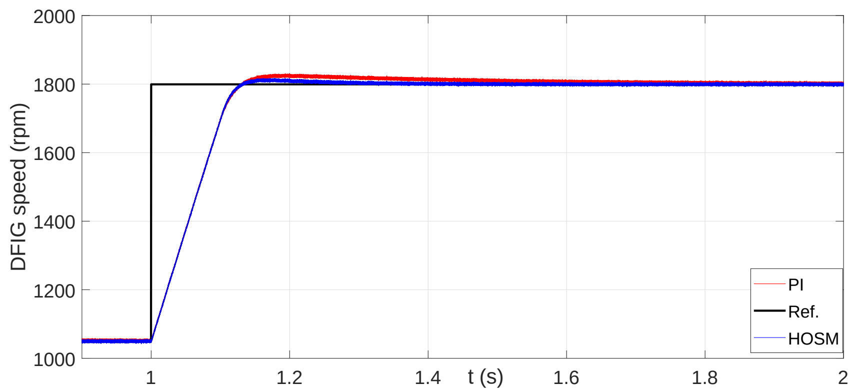

Figure 20: Rotor speed regulation using the traditional PI controller and the proposed HOSM

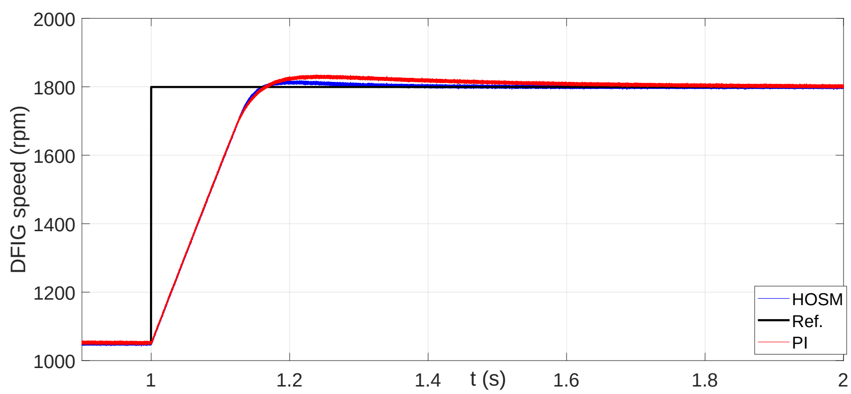

Figure 21: Rotor speed regulation using the traditional PI controller and the proposed HOSM when J increases 25%.

tained with this new value of the system inertia using both controllers, the PID and the proposed HOSM. It can be appreciated in the figure that the rising time increases for both controllers due to the increment in the system inertia. However, this variation in the system parameters increases the overshoot and the settling time in the PID controller, which implies a worse tracking and therefore a lower performance of this control scheme. On the contrary, due to the robustness properties of the HOSM, the performance of this control scheme is not deteriorated.

6. Conclusion

This paper presented a HOSM control scheme for a DFIG used in a variable speed wind turbine system. The aforementioned approach achieved an optimal power efficiency of the turbine operation over a wide range of wind speed in the presence of system uncertainties.

The proposed control scheme includes an HOSM aerodynamic torque observer in order to avoid the need for wind speed measurements, which are typically required in order to calculate the turbine reference speed for maximizing wind power capture. The stability of this HOSM observer has been proved through Lyapunov stability theory.

Due to the nature of the HOSM control, the proposed control scheme avoids the chattering phenomenon, which usually appears in the traditional sliding mode control due to the discontinuity in the control signal, whilst maintaining the robustness under the system uncertainties and wind speed variations.

The proposed approach allows the operation of a wind turbine over a wide range of values for the wind speed while optimizing power efficiency. This controller regulates the speed of the wind turbine by obtaining the optimal tip speed ratio, and consequently, producing the maximum power.

Experimental tests, developed in a real test bench, specifically designed and constructed for this experimental validation, prove that the proposed control method controls efficiently and successfully the variable speed wind turbine within differing wind speed conditions.

The experimental validation demonstrates that the proposed HOSM observer and controller provide both a good estimation of the aerodynamic torque as well as that the speed tracking objective is achieved, in order to maintain the maximum power extraction, under wind speed variations and system uncertainties.

Acknowledgment

The authors are very grateful to the Basque Government by its support through the project SMAR3NAK (ELKARTEK KK-2019/00051), to the Diputación Foral de Álava (DFA) by its support through the project CONAVAUTIN 2, to Gipuzkoako Foru Aldundia by its support through the project Etorkizuna Eraikiz 2019, and to the UPV/EHU by its support through the project PPGA20/06.

References

[1] World Wind Energy Association World Wind Energy Report 2018, WWEA Head Office 2019. Bonn, Germany.

[2] Global wind report 2018, April 2019. Global Wind Energy Council. GWEC Head Office 2019. Brussels, Belgium. https://gwec.net/wp-content/uploads/2019/04/GWEC-Global-Wind-Report-2018.

[3] Ghulam Sarwar Kaloi, Jie Wang, and Mazhar Hussain Baloch, Active and reactive power control of the doubly fed induction generator based on wind energy conversion system Energy Reports, 2016, vol. 2, pp. 194-200.

[4] Shanzhi Li, Haoping Wang, Abdel Aitouche, Nicolai Christov. Active fault tolerant control of wind turbine systems based on DFIG with actuator fault and disturbance using Takagi–Sugeno fuzzy model. Journal of the Franklin Institute, 355 (16) (2018) 8194-8212.

[5] Andreas Giannakis, Athanasios Karlis, Yannis L. Karnavas. A combined control strategy of a DFIG based on a sensorless power control through modified phase-locked loop and fuzzy logic controllers. Renewable Energy 2018;121:489-501.

[6] G. Rigatos, P. Siano, M. Abbaszadeh, P. Wira. Nonlinear optimal control for wind power generators comprising a multi-mass drivetrain and a DFIG. Journal of the Franklin Institute, 356 (5) (2019) 2582-2605.

[7] Oscar Barambones, Jose A. Cortajarena, Isidro Calvo, Jose M. Gonzalez de Durana, Patxi Alkorta and A. Karami-Mollaee, Variable speed wind turbine control scheme using a robust wind torque estimation, Renewable Energy, 133 (2019) 354-366.

[8] Wei Qiao, Wei Zhou, José M. Aller, and Ronald G. Harley, Wind Speed Estimation Based Sensorless Output Maximization Control for a Wind Turbine Driving a DFIG, IEEE Trans. on Power Electronics, 23 (3) (2008) 1156-1169.

[9] Shi F. and R. J. Patton, An active fault tolerant control approach to an offshore wind turbine Model, Renewable Energy, 75 (2015) 788–798.

[10] Evangelista C., Pisano A., Puleston P., Usai E, Conventional and adaptive second-order sliding mode control of a wind energy conversion system , in Recent Trends in Sliding Mode Control. The Institution of Engineering and Technology. 2016.

[11] M. L. Corradini, G. Ippoliti, G. Orlando. Fault-tolerant sensorless control of wind turbines achieving efficiency maximization in the presence of electrical faults. Journal of the Franklin Institute, 355 (5) (2018) 2266-2282.

[12] Larbi Djilali, Edgar N. Sanchez , Mohammed Belkheiri. Real-time Neural Input–Output Feedback Linearization control of DFIG based wind turbines in presence of grid disturbances. Control Engineering Practice, 83 (2019) 151–164.

[13] Kamyar Ghanbarpour, Farhad Bayat, Abolfazl Jalilvand. Dependable power extraction in wind turbines using model predictive fault tolerant control. Electrical Power and Energy Systems, 118 (2020) 105802

[14] Linyun Xiong, Penghan Li, Fei Wu, Meiling Ma, Muhammad Waseem Khan, Jie Wang. A coordinated high-order sliding mode control of DFIG wind turbine for power optimization and grid synchronization. Electrical Power and Energy Systems, 105 (2019) 679–689.

[15] Jován Mérida, Luis T. Aguilar, Jorge Dávila. Analysis and synthesis of sliding mode control for large scale variable speed wind turbine for power optimization. Renewable Energy, 71 (2014) 715-728.

[16] Yifang Liu, Zhijie Wang, Linyun Xiong, Jie Wang, Xiuchen Jiang, Gehao Bai, Renfu Li ,Sanming Liu. DFIG wind turbine sliding mode control with exponential reaching law under variable wind speed. Electrical Power and Energy Systems, 96 (2018) 253–260

[17] Juan J. Ley-Rosas, Luis E. González-Jiménez, Alexander G. Loukianov, Jorge E. Ruiz-Duarte. Observer based sliding mode controller for vehicles with roll dynamics. Journal of the Franklin Institute, 356 (5) (2019) 2559-2581.

[18] C. Edwards, Y. Shtessel. Enhanced continuous higher order sliding mode control with adaptation. Journal of the Franklin Institute, 356 (9) (2019) 4773-4784.

[19] José Antonio Cortajarena, Oscar Barambones, Patxi Alkorta, Julián De Marcos, Sliding mode control of grid-tied single-phase inverter in a photovoltaic MPPT application, Solar Energy 155 (2017) 793–804.

[20] Maissa Farhat, Oscar Barambones and Lassaad Sbita. A New Maximum Power Point Method Based on a Sliding Mode Approach for Solar Energy Harvesting. Applied Energy. 185 (2017) 1185-1198.

[21] Oscar Barambones, José A. Cortajarena, José M. Gonzalez de Durana, Patxi Alkorta, A real time sliding mode control for a wave energy converter based on a wells turbine, Ocean Engineering 163 (2018) 275–287.

[22] O. Barambones and J.M. Gonzalez de Durana, Second Order Sliding Mode Controller and Observer for a Wind Turbine System, IEEE International Conference on Enviroment and Electrical Engineering. 2017 pp.133-138.

[23] Vladislav Akhmatov, Variable-Speed Wind Turbines with Doubly-Fed Induction Generators,Wind Engineering, 26 (2) (2002) 85–108.

[24] Fernando D. Bianchi, Hérnan De Battista and Ricardo J. Mantz, Wind Turbine Control Systems Advances in Industrial Control Series. Springer. 2007.

[25] Y.D. Song, B. Dhinakaran, X.Y. Bao, Variable speed control of wind turbines using nonlinear and adaptive algorithms, Journal of Wind Engineering and Industrial Aerodynamics, 85 (2000) 293-308.

[26] R. Pena, J. C. Clare, and G. M. Asher, Doubly fed induction generator using back-to-back PWM converters and its application to variablespeed wind-energy generation Proc. Inst. Elect. Eng., 143 (3) (1996) 231–241.

[27] Oestergaard K., P. Brath and J. Stoustrup, Estimation of effective wind speed, Journal of Physics: Conference Series, 75 (13) (2007) 1-9.

[28] Odgaard P. F. and J. Larsen, Power and Speed Control of Wind Turbines using Rotor Speed Estimates, in Proceedings of EWEA 2011, Bruxelles.

[29] Levant, A., Sliding order and sliding accuracy in sliding mode control, Int. J. Control, 58 (6) (1993) 1247–1263.

[30] J. A. Moreno, M. Osorio, A Lyapunov approach to second-order sliding mode controllers and observers, 47th IEEE Conference on Decision and Control, Cancun, Mexico, 2008 pp. 2866-2861.

[31] Yazhou Lei, Alan Mullane, Gordon Lightbody, and Robert Yacamini, Modeling of the Wind Turbine With a Doubly Fed Induction Generator for Grid Integration Studies, IEEE Trans. on Energy Conversion, 21 (1) (2006) 257-264.

[32] G.M. Joselin Herbert, S. Iniyan, E. Sreevalsan, S. Rajapandian, A review of wind energy technologies, *Renewable and Sustainable Energy Reviews*, 11 (2007) 1117–1145.

[33] Siegfried Heier, Grid Integration of Wind Energy Conversion Systems John Wiley & Sons Ltd, 1998, ISBN 0-471-97143-X.

[34] G. Bartolini A. Ferrara, A. Levant, E. Usai, On second order sliding mode controllers," in Variable structure systems, sliding mode and nonlinear control. Springer-Verlag, 1999 pp.329-350.

[35] Fridman L. and Levant A., Sliding Mode Control in Engineering. New York: Marcel Dekker, 2002, ch. 3, pp. 53–101.

[36] A. Levant, Principles of 2-sliding mode design. Automatica, (2007) 43, 576–586.

[37] Fridman L., Moreno.J. and Iriarte R., Sliding Modes after the First Decade of the 21st Century. Lecture Notes in Control and Information Sciences book series, 412, (2011). ch.1 pp. 3–49.

[38] Ashpana Shiralkar and Shailaja Kurode , Generalized Super-Twisting Algorithm for Control of Electro-Hydraulic Servo System. IFAC-PapersOnLine 49-1 (2016) 742–747.

[39] Aitor Saenz-Aguirre, Unai Fernandez-Gamiz, Ekaitz Zulueta, Alain Ulazia and Jon Martinez-Rico. OptimalWind Turbine Operation by Artificial Neural Network-Based Active Gurney Flap Flow Control, Sustainability, 11 (2019) 1-17.